Supporting Information

Nature of Sulfonyl Deactivation/Activation by Metal Catalysts

Zhihui Li,[a] Lanbo Liu,[a] Wan Li,[a] Xueqing Song,[a]* Zheng Wang,[b]* Longfei Li[a]*

[a] *College of Pharmacy, Key Laboratory of Pharmaceutical Quality Control of Hebei Province, Key Laboratory of Medicinal Chemistry and Molecular Diagnosis of Ministry of Education, Hebei University, Baoding 071002, Hebei, P. R. China*

[b] *College of Science, Hebei Agricultural University, Baoding 071001, Hebei, P. R. China*

*Email: lilongfei@hbu.edu.cn (L.L.), sxqing@hbu.edu.cn (X.S.), wangzheng@iccas.ac.cn (Z.W.)

Table S1. The computed potential energies (E, a.u.) and free energies (ΔG; at 423.15 K) are in kcal/mol at the ωB97X-D/BS-II level.

Complex	E	G	ΔG
Mn1	-1669.1480	-1668.8768	0.0
Mn2	-2015.9507	-2015.5584	2.1
Mn3	-2015.9600	-2015.5682	-4.0
Mn4	-2015.9261	-2015.5346	17.1
Mn5	-1670.3537	-1670.0614	2.4
TSMn1–4	-2015.9153	-2015.5275	21.5
TSMn2–3	-2015.9275	-2015.5427	12.0
TSMn3–4	-2015.9147	-2015.5237	24.0
TSMn4–5	-2015.9240	-2015.5364	15.9
4	-1058.3366	-1058.2468	11.1
5	-1058.3191	-1058.2336	19.4
6	-981.8558	-981.7881	21.0
7	-1327.4699	-1327.3012	10.6
8	-1403.9318	-1403.7447	10.3
9	-1403.9297	-1403.7417	12.2
10	-1327.4470	-1327.2810	23.3
11	-1327.4507	-1327.2883	18.7
12	-1089.2845	-1089.1288	8.6
13	-1327.4084	-1327.2433	46.9
14	-309.6289	-309.5432	-21.2
TS4–5	-1058.3191	-1058.2342	19.1
TS8–9	-1403.9286	-1403.7429	11.4
TS9–10	-1403.9043	-1403.7201	25.7
TS10–11	-1327.4350	-1327.2758	26.6
TS13–14	-1327.3875	-1327.2217	60.5
Mn6*α*	-2759.6555	-2759.1713	20.5
Mn6*β*	-2759.6532	-2759.1692	21.8
Mn7*β*	-2759.6789	-2759.1921	7.5
Mn8	-2759.7022	-2759.2175	-8.5
Mn9	-2450.0708	-2449.7063	-28.6
Mn10	-1745.6121	-1745.2763	-32.0
TSMn5–6*α*	-2759.6399	-2759.1556	30.3
TSMn5–6*β*	-2759.6433	-2759.1602	27.4
TSMn7*β*–8	-2759.6634	-2759.1831	13.1
TSMn10–1	-1745.5864	-1745.2533	-16.8
TSMn5–6*α*_CH_3	-2567.9043	-2567.4655	38.0
TSMn5–6*β*_CH_3	-2567.9168	-2567.4792	29.4
TSMn5–6*α*_H	-2528.5835	-2528.1710	37.5
TSMn5–6*β*_H	-2528.5982	-2528.1849	28.7
TSMn5–6*α*_OMe	-2874.1629	-2873.6509	30.8
TSMn5–6*β*_OMe	-2874.1681	-2873.6592	25.6

TSMn5–6*α*_C_6F_5	-3255.8302	-3255.3977	25.0
TSMn5–6*β*_C_6F_5	-3255.8272	-3255.3920	28.5
Mn1^{triplet}	-1669.1326	-1668.8686	5.1
Mn2^{triplet}	-2015.8895	-2015.5060	35.1
Mn3^{triplet}	-2015.9238	-2015.5363	16.0
Mn4^{triplet}	-2015.8929	-2015.5097	32.7
Mn5^{triplet}	-1670.3128	-1670.0282	23.3
TSMn2–3^{triplet}	-2015.8732	-2015.4925	43.5
TSMn3–4^{triplet}	-2015.8919	-2015.5086	33.4
TSMn4–5^{triplet}	-2015.8775	-2015.5007	38.4
TSMn5–6*α*_2	-2759.6354	-2759.1538	31.5
TSMn5–6*β*_2	-2759.6421	-2759.1560	30.1
Mn11*α*	-2759.6969	-2759.2024	0.9
Mn11*β*	-2759.6961	-2759.2044	-0.3
Mn12	-1670.3068	-1670.0183	35.7
Mn13	-2759.6179	-2759.1324	44.9
Mn14	-2759.6122	-2759.1283	47.4
TSMn6*α*–1	-2759.6407	-2759.1579	28.9
TSMn6*β*–1	-2759.6477	-2759.1625	26.0
TSMn11*α*–1	-2759.6524	-2759.1662	23.7
TSMn11*β*–1	-2759.6437	-2759.1586	28.5
Mn15	-1979.2841	-1978.8736	13.3
Mn16	-2450.0761	-2449.7081	-29.7
TSMn6*α*–15	-2759.6448	-2759.1629	25.7
TSMn11*α*–15	-2759.6665	-2759.1813	14.2
TSMn5–6*α*_NH_2	-2870.3793	-2869.8655	30.4
TSMn5–6*β*_NH_2	-2870.3804	-2869.8718	26.4
TSMn5–6*α*_F	-2958.1319	-2957.6663	30.4
TSMn5–6*β*_F	-2958.1306	-2957.6684	29.1

Table S2. The imaginary frequencies (in cm^{-1}) of transition states at the ωB97X-D/BS-I level.

Complex	Imaginary frequencies (in cm^{-1})
TSMn1–4	1180.8*i*
TSMn2–3	1424.8*i*
TSMn3–4	267.9*i*
TSMn4–5	321.3*i*
TS4–5	716.5*i*
TS8–9	506.4*i*
TS9–10	999.2*i*
TS11–12	117.3*i*
TS13–14	284.7*i*
TSMn5–6*α*	715.3*i*
TSMn5–6*β*	692.0*i*
TSMn7*β*–8	1341.1*i*
TSMn6*β*–1	1202.8*i*
TSMn10–1	1444.3*i*
TSMn5–6*α*_CH_3	726.0*i*
TSMn5–6*β*_CH_3	546.5*i*
TSMn5–6*α*_H	707.4*i*
TSMn5–6*β*_H	521.3*i*
TSMn5–6*α*_OCH_3	751.8*i*
TSMn5–6*β*_OCH_3	772.0*i*
TSMn5–6*α*_C_6F_5	413.4*i*
TSMn5–6*β*_C_6F_5	690.5*i*
TSMn2–3^{triplet}	1358.8*i*
TSMn3–4^{triplet}	35.9*i*
TSMn4–5^{triplet}	344.0*i*
TSMn5–6*α*_2	779.8*i*
TSMn5–6*β*_2	813.5*i*
TSMn6*α*–1	1267.1*i*
TSMn11*α*–1	1493.3*i*
TSMn6*β*–1	1202.8*i*
TSMn11*β*–1	1326.6*i*
TSMn6*α*–15	203.8*i*
TSMn11*α*–15	196.7*i*
TSMn5–6*α*_NH_2	624.4*i*
TSMn5–6*β*_NH2	659.9*i*
TSMn5–6*α*_F	712.6*i*
TSMn5–6*β*_F	683.5*i*

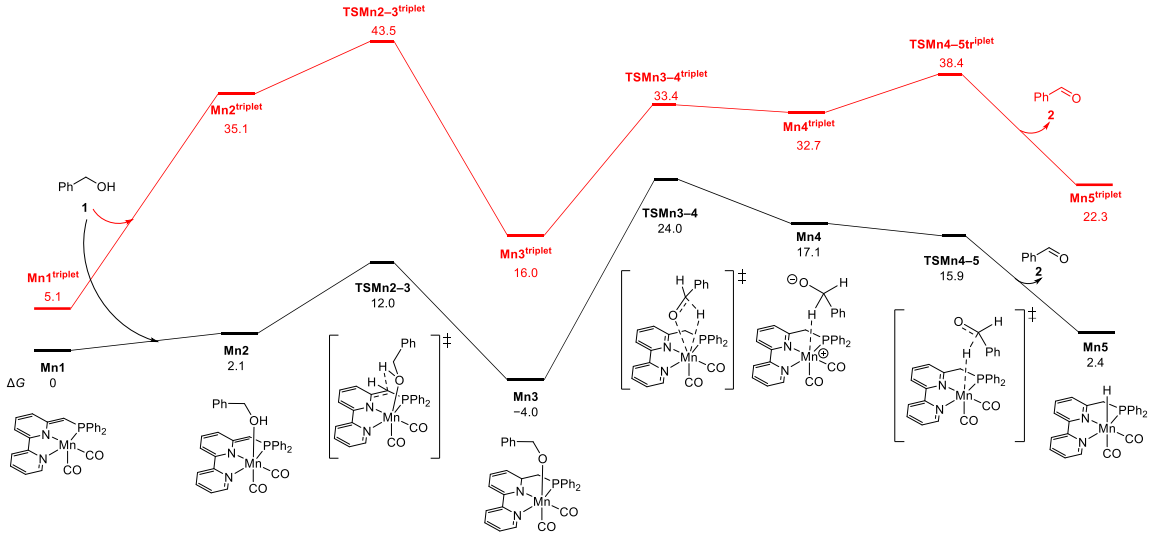

Figure S1. The comparisons of triplet and singlet states for Mn complexes in the bifunctional dehydrogenation of benzyl alcohol at the ωB97X-D/SDD[6-311++G(2d, p)]//ωB97X-D/SDD[6-311G(d, p)] level. The relative free energies (ΔG) are in kcal/mol. The n/a denotes the structure can not be located.

The triplet states (red line) and singlet states (black line) of the bipyridine-based manganese pincer complexes involved in the bifunctional dehydrogenation of benzyl alcohol are compared in Figure S1. The red line lies above the black line. Therefore, the manganese pincer complexes adopt the singlet ground state.

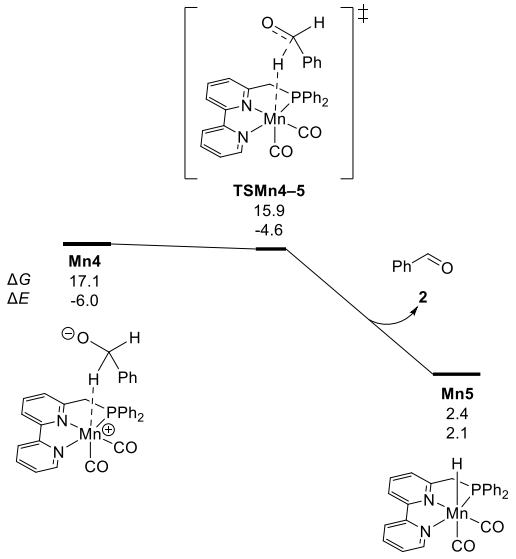

Figure S2. The energy profile for the hydride transfer step via transition state **TSMn4–5** at the ωB97X-D/SDD[6-311++G(2d, p)]//ωB97X-D/SDD[6-311G(d, p)] level. The relative free energies (ΔG) and potential energies (ΔE) are in kcal/mol.

As shown in Figure S2, although the free energy of transition state **TSMn4–5** appears to be lower than that of **Mn4**, the potential energy of **TSMn4–5** is higher than that of **Mn4**.

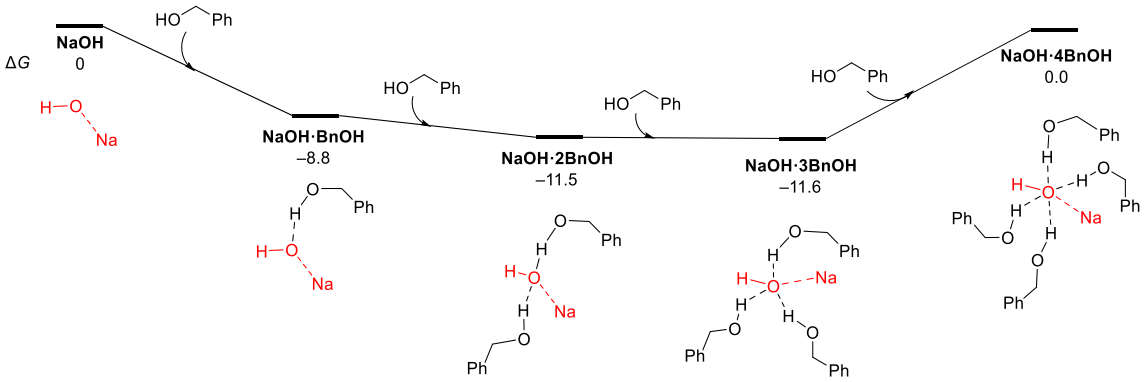

(a)

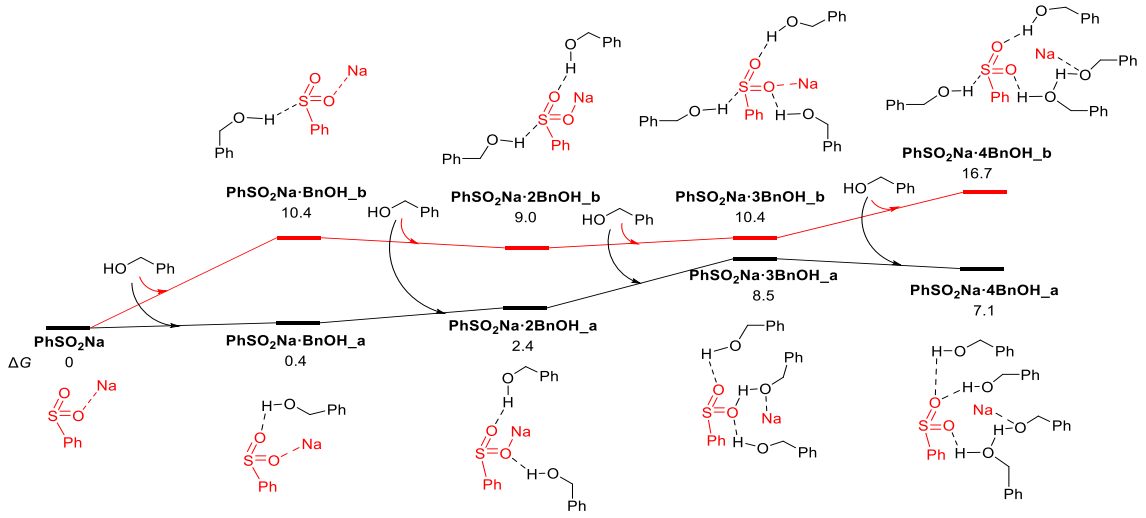

(b)

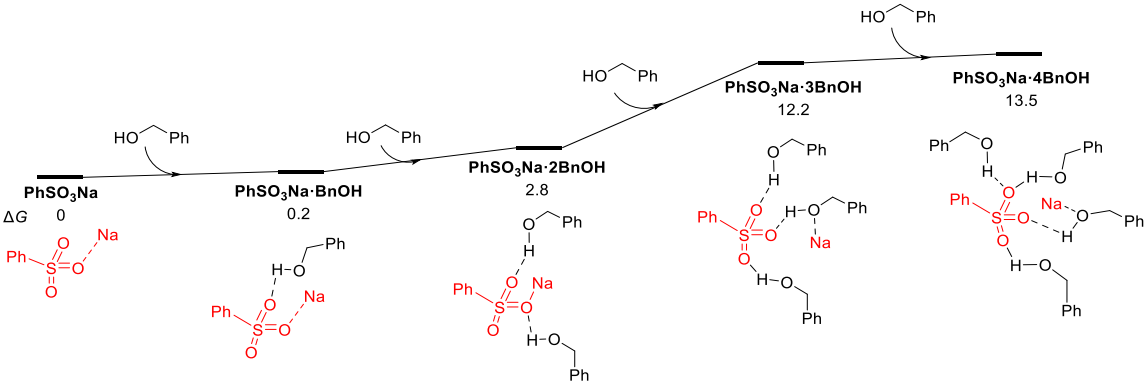

(c)

Figure S3. The preferential solvation of NaOH, $PhSO_2Na$, $PhSO_3Na$ with benzyl alcohol at the ωB97X-D/6-311++G(2d, p)//ωB97X-D/ 6-311G(d, p) level. The relative free energies (ΔG) are in kcal/mol.

In accordance with NaOH-catalyzed mechanisms,[1-5] the preferential solvation of NaOH with the benzyl alcohol (BnOH) is considered in Figure S3. The NaOH can approach the benzyl alcohol molecule through hydrogen-bonding interactions and generate the complex **NaOH·BnOH** with being exothermic by 8.8 kcal/mol. If more benzyl alcohol molecules are added, the process will further be exothermic until the fourth benzyl alcohol molecules. Therefore, the **NaOH·3BnOH** complex with three BnOH molecules is most stable in the presence of benzyl alcohol.

In contrast, the additions of BnOH into $PhSO_2Na$ are predicted to be endergonic, suggesting $PhSO_2Na$ can not form stable complex with BnOH. The additions of BnOH into $PhSO_3Na$ are predicted to be endergonic, suggesting $PhSO_3Na$ can not form stable complex with BnOH.

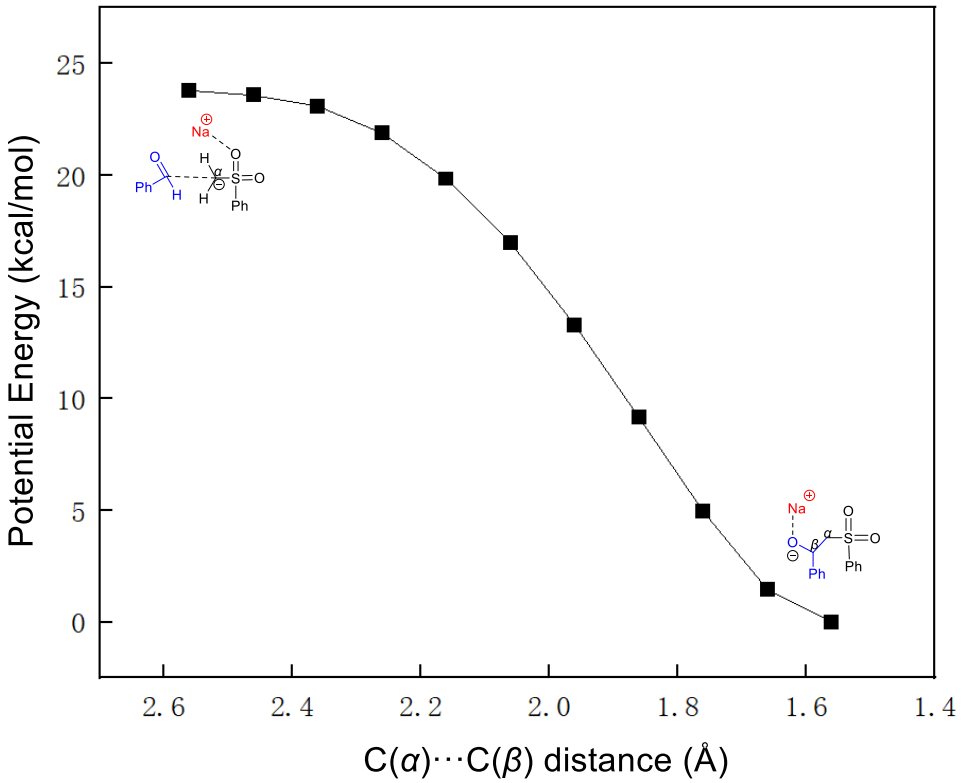

Figure S4. The relaxed potential energies surface scan along the C(α)···C(β) distance for the C−C coupling step.

The relaxed potential energies surface scan is performed as shown in Figure S4 and suggests the C−C coupling between the ionic intermediate **6** and benzaldehyde **2** is a spontaneous step without energy barrier.

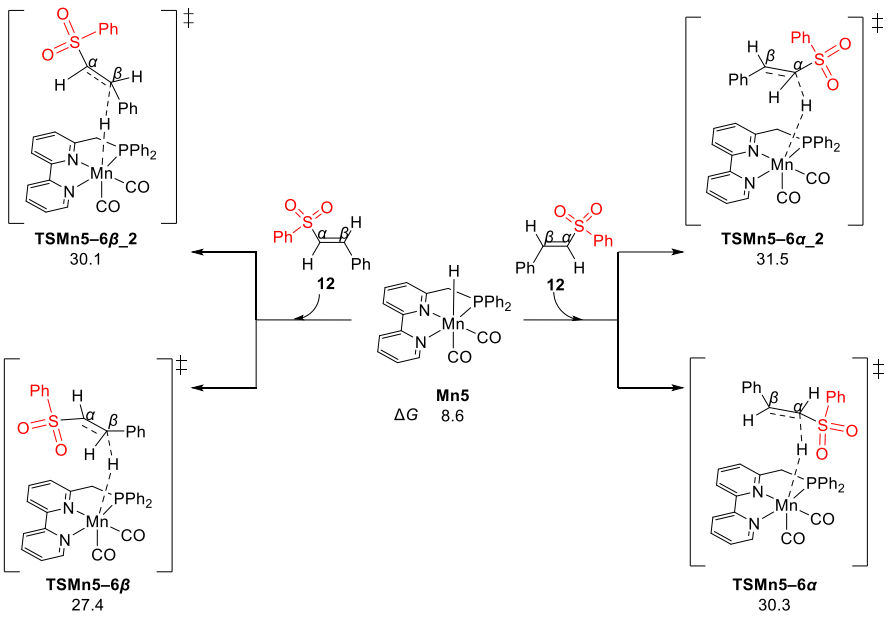

Figure S5. The possible transition states of the hydride addition step in the bifunctional outershpere C=C hydrogenation at the ωB97X-D/SDD[6-311++G(2d, p)]//ωB97X-D/SDD[6-311G(d, p)] level. The relative free energies (Δ*G*) are in kcal/mol.

The possibility of the hydride transfers from the Mn center to the *β*-C atom of vinyl sulfone molecule **12** is considered in Figure S5. Through the transition state **TSMn5–6*β***, the hydride transfers from the Mn center to the *β*-C atom of vinyl sulfone molecule, and the energy barrier for this step is 18.8 kcal/mol. Through the transition state **TSMn5–6*β*_2**, the hydride transfers from the Mn center to the *β*-C atom of vinyl sulfone molecule, and the energy barrier for this step is 21.5 kcal/mol. The hydride of **Mn5** can transfer to the *α*-C atom of vinyl sulfone molecule through the transition state **TSMn5–6*α***, and the energy barrier for this step is 21.7 kcal/mol. Alternatively, through the transition state **TSMn5–6*α*_2**, the hydride transfers from the Mn center to the *α*-C atom of vinyl sulfone molecule, and the energy barrier for this step is 22.9 kcal/mol. As for the hydride transfer transition states, the energy barrier for **TSMn5–6*β*** is lower than those for **TSMn5–6*α***, **TSMn5–6*α*_2** and **TSMn5–6*β*_2**, suggesting the pathway with the terminal *β*-C atom as the hydride acceptor is most favorable.

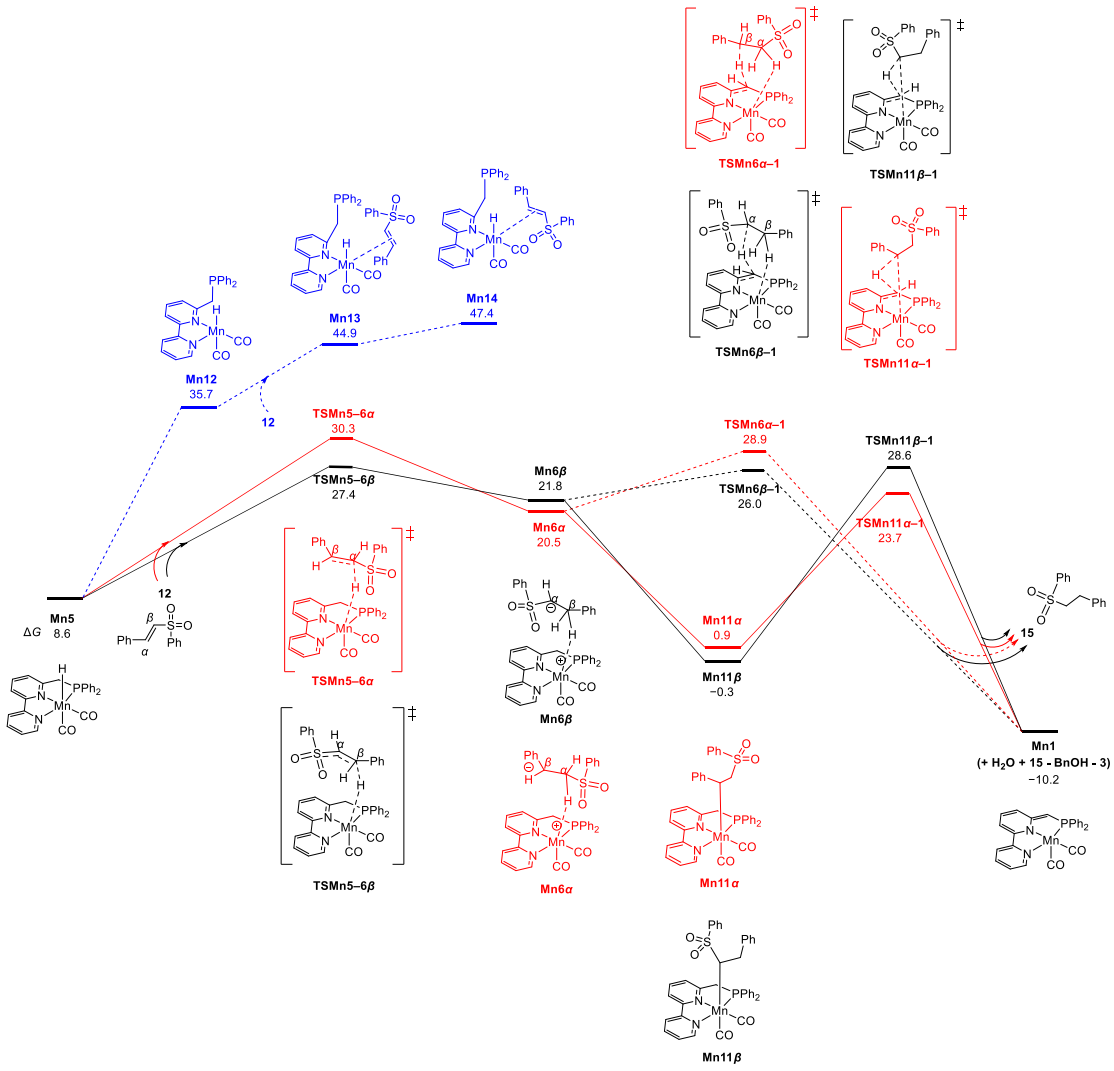

Figure S6. The unfavorable pathways for the C=C hydrogenation stage at the ωB97X-D/SDD[6-311++G(2d, p)]//ωB97X-D/SDD[6-311G(d, p)] level. The relative free energies (ΔG) are in kcal/mol.

As shown in Figure S6, the black dotted line features the outersphere proton transfer over the transition state **TSMn6*β*–1**. The red lines denote the pathway with the hydride transfer into the α-C atom over the transition state **TSMn5–6*α***. The blue line denotes the innersphere pathway, but the substitution of phosphine ligand of **Mn5** by the C=C bond of vinyl sulfone will form very unstable intermediates **Mn13** and **Mn14** which are

inaccessible at experimental temperatures. These pathways are less favorable than the pathway in maintext.

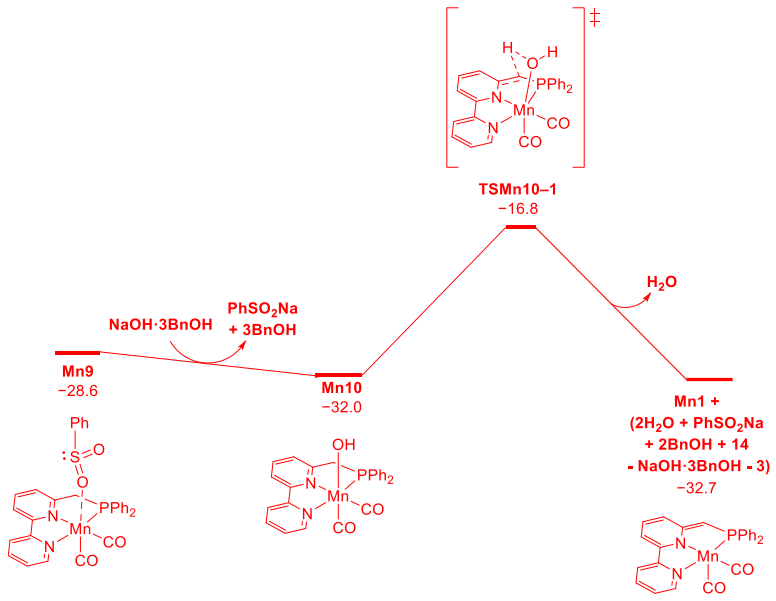

Figure S7. The dehydration process via the aromatization−dearomatization metal–ligand cooperation at the ωB97X-D/SDD[6-311++G(2d, p)]//ωB97X-D/SDD[6-311G(d, p)] level. The relative free energies (ΔG) are in kcal/mol.

As shown in the Figure S7, the **Mn10** undergoes the dehydration process via the aromatization−dearomatization metal–ligand cooperation, and regenerates the catalytic species Mn1 through transition state **TSMn10–1** with an energy barrier of 15.2 kcal/mol.

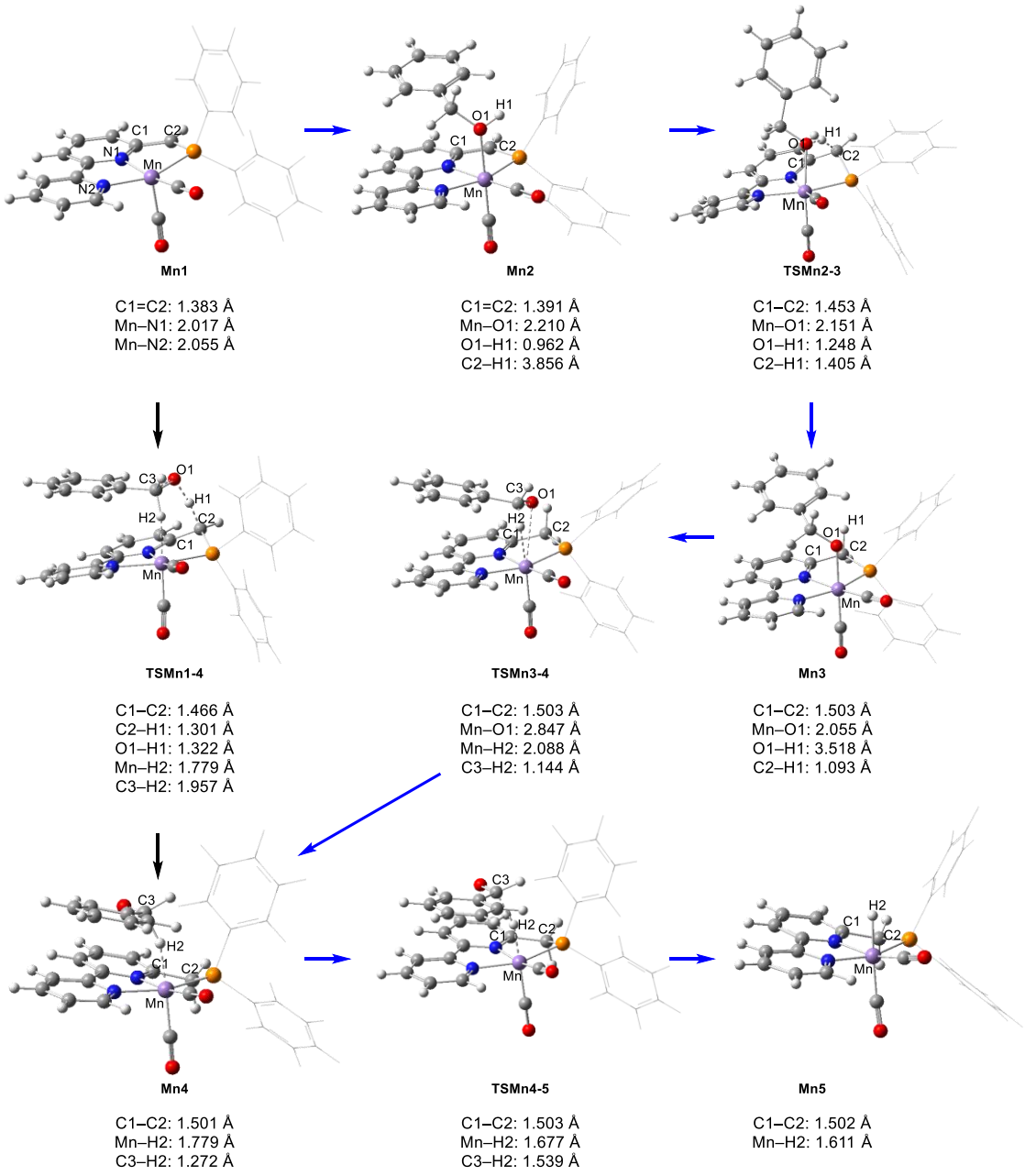

Figure S8. Optimized geometries of Mn species involved in Figure 2. The $-PPh_2$ groups are drawn in wireframe for simplicity.

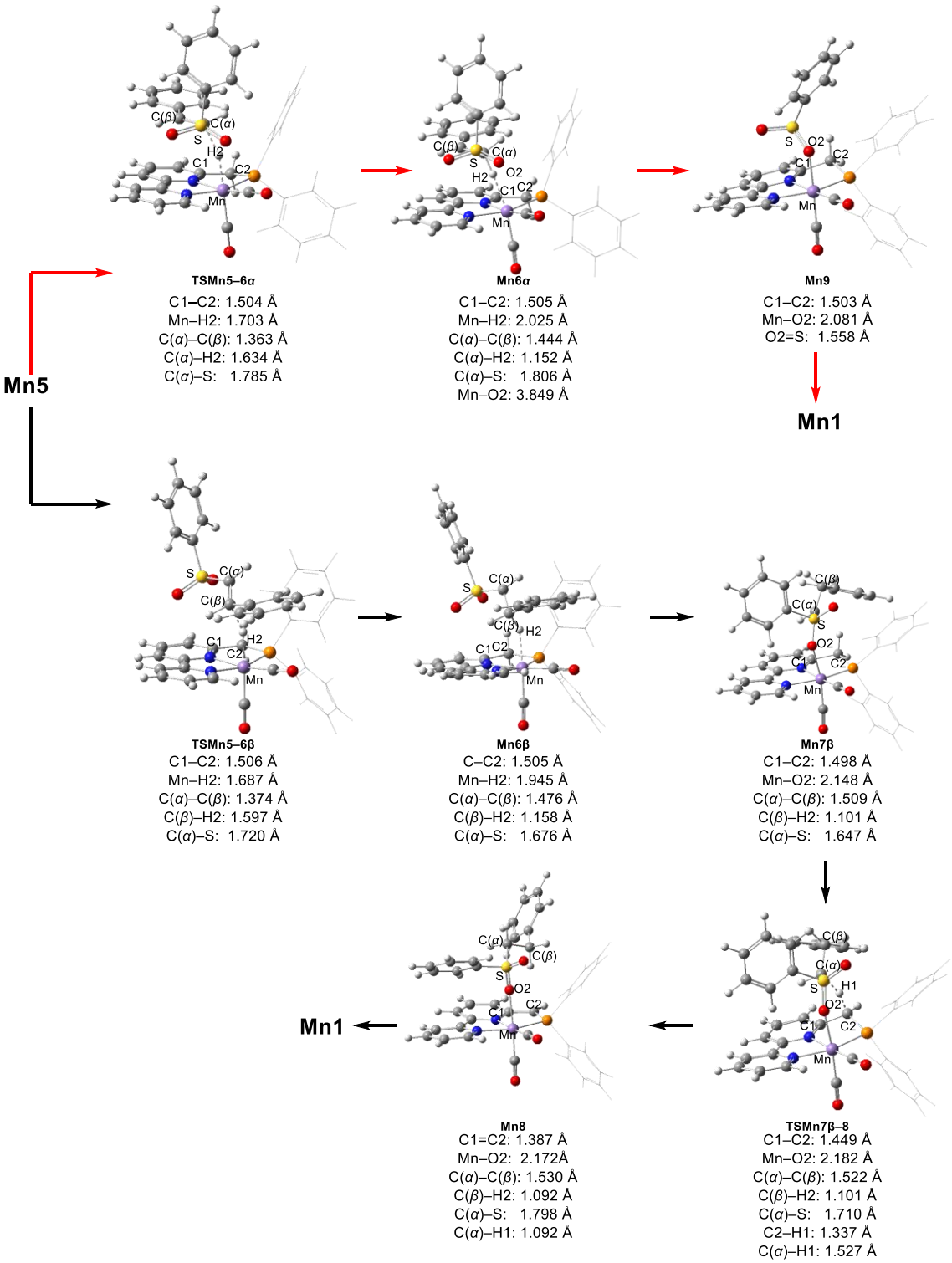

Figure S9. Optimized geometries of Mn species involved in Figure 4. The $-PPh_2$ groups are drawn in wireframe for simplicity.

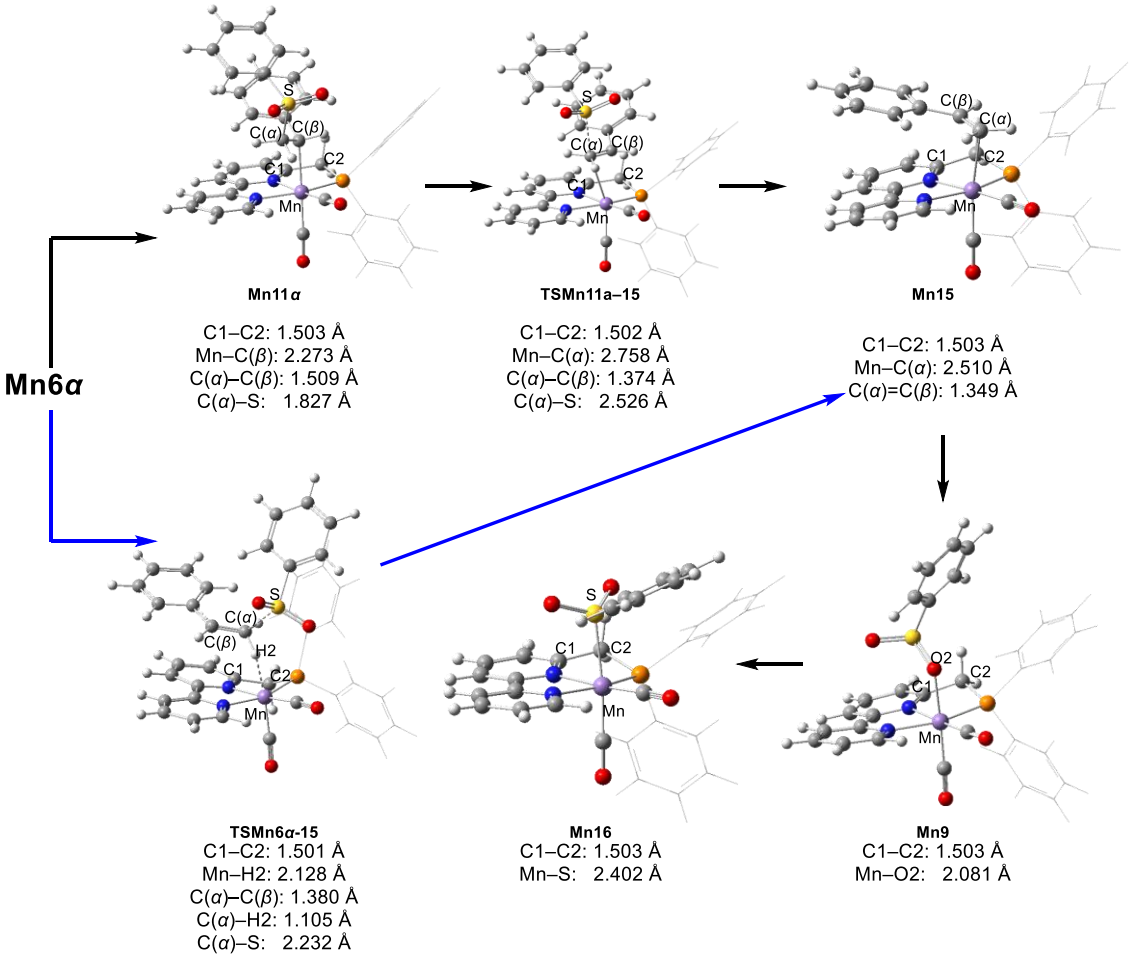

Figure S10. Optimized geometries of Mn species involved in Figure 5. The −PPh_2 groups are drawn in wireframe for simplicity.

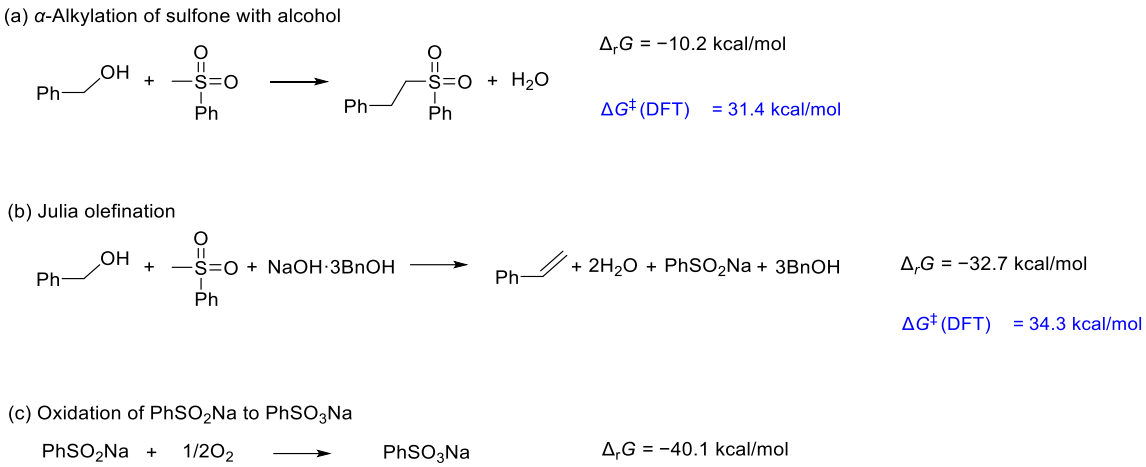

Figure S11. The thermodynamical and dynamical comparisons for (a) α-alkylation of sulfone with alcohol, (b) Julia olefination, and (c) oxidation of $PhSO_2Na$ to $PhSO_3Na$.

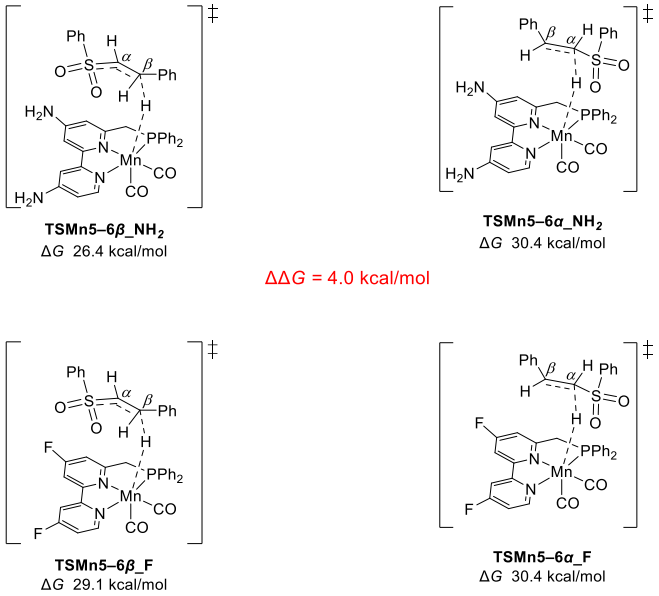

Figure S12. The pincer ligand modulations for the chemoselectivity-determining hydride addition transition states at the ωB97X-D/SDD[6-311++G(2d, p)]//ωB97X-D/SDD[6-311G(d, p)] level.

As shown in the Figure S12, the electron-donating NH_2 groups in the bipyridine ring of the pincer ligand increase the $\Delta\Delta G$ to 4 kcal/mol with increasing the selectivity for the α-alkylation products. However, the electron-withdrawing F groups in the bipyridine ring of the pincer ligand decrease the $\Delta\Delta G$. This could unveil that the hydride addition into the C(β) atom is more sensitive to the electronegativity of hydride.

Analysis of the product ratio.

$$\frac{[\alpha\text{-alkylated sulfonyl product}]}{[\text{Julia olefination product}]+[\alpha\text{-alkylated sulfonyl product}]}*100\% = \frac{1}{1+e^{\frac{-\Delta\Delta G^{\neq}}{RT}}}*100\% \qquad (1)$$

$$= \frac{1}{1+e^{\frac{-(2.9*4184\,J/mol)}{8.314\,J/(mol*K)*423.15K}}}*100\%$$

$$= 96.9\%$$

$$\frac{[\alpha\text{-alkylated sulfonyl product}]}{[\text{Julia olefination product}]} = \frac{97}{3}$$

The computed energy difference ($\Delta\Delta G$) has been used to predict the product ratios and enantiomeric excess (ee).[6] Herein, the equation 1 is used to calculate production ratio. The computed energy difference $\Delta\Delta G$ (2.9 kcal/mol) between the rate-determining transition states**TSMn5–6*β*** and **TSMn5–6*α*** corresponds to a 97:3 ratio at 423 K, and it is in good agreement with the experimental ratio 96:4.

Table S3. Summary of the substituent modulations for the chemoselectivity-determining hydride addition **TSMn5-6*β*** and **TSMn5-6*α***.

Complex	*ΔG* (kcal/mol)	*ΔΔG* (kcal/mol)	$E^{(2)}(\pi_{C(\alpha)=C(\beta)} \rightarrow \delta^*_{S-O})$ (kcal/mol)	$E^{(2)}(\pi_{C(\alpha)=C(\beta)} \rightarrow \pi^*_{Ph})$ (kcal/mol)	Product ratio
TSMn5-6*β*	27.4	2.9	9.2	2.4	97:3
TSMn5-6*α*	30.3		2.1	54.7	
TSMn5-6*β*_H	28.7	8.8	7.9	/	100:0
TSMn5-6*α*_H	37.5		/	0	
TSMn5-6*β*_CH_3	29.4	8.6	8.8	/	100:0
TSMn5-6*α*_CH_3	38.0		/	4.6	
TSMn5-6*β*_OMe	25.6	5.2	9.8	/	100:0
TSMn5-6*α*_OMe	30.8		/	54.5	
TSMn5-6*β*_C_6F_5	28.5	-3.5	7.1	/	2:98
TSMn5-6*α*_C_6F_5	25.0		/	64.8	

References

1. E. V. Anslyn and D. A. Dougherty, *Modern physical organic chemistry*, University Science Books: Sausalito, 2006, pp510–515.
2. A. Kumar, M. Park, J. Y. Huh, H. M. Lee and K. S. Kim, *J. Phys. Chem.*, 2006, **110**, 12484–12493.
3. C. Ding, X. Zhou, J. Shi, P. Yan, Z. Wang, G. Liu and C. Li, *J. Phys. Chem. B*, 2015, **119**, 3560−3566.
4. M. Rossa, J. C. Ferrero, I. Cabanillas-Vidosa and C. J. Cobos, *Chem. Phys. Lett.*, 2015, **620**, 19–24.
5. C. Stamou, S. P. Perlepes, M. M. Sigalas, D. Papaioannou, A. C. Tsipis and E. G. Bakalbassis, *J. Org. Chem.*, 2024, **89**, 13894–13912.
6. K. H. Hopmann, *Int. J. Quantum Chem.*, 2015, **115**, 1232−1249.